A&A 418, 539–549 (2004)
DOI: 10.1051/0004-6361:20040043

Astronomy & Astrophysics

Membership, rotation, and lithium abundances in the open clusters NGC 2451 A and B⋆

M. Hünsch[1], S. Randich[2], M. Hempel[3], C. Weidner[1], and J. H. M. M. Schmitt[3]

[1] Institut für Theoretische Physik und Astrophysik, Universität Kiel, Olshausenstraße 40, 24118 Kiel, Germany
[2] INAF–Osservatorio Astrofisico di Arcetri, Largo Fermi 5, 50125 Firenze, Italy
[3] Hamburger Sternwarte, Universität Hamburg, Gojenbergsweg 112, 21029 Hamburg, Germany

Received 19 June 2003 / Accepted 15 January 2004

Abstract. High-resolution spectra of 30 late-type and 9 early-type candidate members of the young (∼50–80 Myr) open clusters NGC 2451 A and B have been analyzed in order to complement our previous photometric and X-ray study. Cluster membership of these X-ray selected stars has been confirmed or rejected on the basis of radial velocity and Hα chromospheric emission. The metallicity of both clusters seems to be about solar – contrary to previous investigations. Lithium abundances have been determined by two different methods, namely curve-of-growth techniques and spectrum synthesis, yielding quite consistent results. The pattern of Li abundances versus effective temperature resembles that of the equally-old Alpha Per cluster, i.e., little Li depletion is seen for solar–type and earlier–type stars, while towards cooler stars Li is more and more depleted, possibly showing a star-to-star scatter below ∼5200 K. The hottest star in our sample shows a Li abundance ∼0.5 dex higher than the meteoritic value. Rotational velocities have been determined in order to investigate the supposed dependence of activity and Li depletion on rotation.

Key words. stars: abundances – stars: late-type – stars: rotation – Galaxy: open clusters and associations: individual: NGC 2451

1. Introduction

Stellar clusters provide homogeneous stellar samples for the study of the age-, mass-, and metallicity-dependence of activity, rotation and light element abundances. About two dozens of the most nearby clusters have been well investigated during the last decade by means of X-ray and optical photometric and spectroscopic observations. A rather good understanding of these issues has been achieved in the context of the so-called age-rotation-activity-paradigm, although various questions are still not settled.

A point of special concern is the evolution of lithium; this element is quickly destroyed by thermonuclear reactions in stellar interiors. According to standard models, i.e., those involving convection as the only mixing mechanism, the Li content should depend only on mass, age, and chemical composition, and similar stars in the same cluster should have the same Li content. It is now well established that standard models are not able to fully reproduce the empirical scenario produced by observations of cluster and field stars. In particular, a large star-to-star scatter in Li abundances is seen among otherwise similar late G- and K- type stars in several young clusters (ages ≤250 Myr). Therefore, extra mixing processes and/or mechanisms which prevent Li destruction must be taken into account in the models. Due to the observed Li–rotation relationship, the most commonly accepted view is that Li depletion is affected by rotation, and that the extra-mixing mechanism is induced by angular momentum loss and angular momentum transport between the surface and the core. For details, we refer to the most recent reviews by Deliyannis (2000), Jeffries (2000), and Pasquini (2000). The issue of the scatter is, however, not settled; for example, there is a debate whether the observed dispersion in Li abundances really reflects a scatter in abundances, or whether other parameters like magnetic activity could affect the measured Li line strengths via, e.g., temperature effects (e.g., Jeffries 1999; Stuik et al. 2000; Randich 2001). Additional studies of nearby young clusters are thus warranted.

In this paper we present spectroscopic observations of the open clusters NGC 2451 A and B, which are accidentally located along the same line of sight at distances of 206 and 370 pc, respectively. A detailed X-ray and photometric study of these two clusters has recently been published by Hünsch et al. (2003 – hereafter HWS). From isochrone fitting and a comparison of their mean X-ray properties with other clusters, both NGC 2451 clusters are estimated to have an age of ≈50 Myr, the nearer cluster A perhaps being slightly older than the more distant cluster B. NGC 2451 deserves special attention as it was originally thought to have significant lower metallicity than the Sun. Lyngå & Wramdemark (1984) derived from

Send offprint requests to: M. Hünsch,
e-mail: mhuensch@astrophysik.uni-kiel.de

⋆ Based on observations performed at the European Southern Observatory, La Silla/Chile.

uvbyβ photometry a value of [metals/H] = −0.5, but were unaware of the true nature of the cluster(s) and possibly observed non-member stars.

High-resolution spectra of selected cluster member candidates provide crucial information on the following items: i) radial velocities, which serve as an additional criterion for cluster membership; ii) Hα emission as an (additional) indicator for activity and thus also membership; iii) metallicity, derived from the abundance determination of iron; iv) rotational velocities, and v) lithium abundances.

2. Observations

High-resolution spectroscopy has been carried out at the ESO/La Silla 1.5 m telescope during 9 half nights between 22 and 31 December 2001. The fibre-feed FEROS echelle spectrograph used for the observations provides a resolution of R = 48 000 over the whole visual wavelength range (3560–9200 Å). A 2048 × 4096 EEV CCD detector with 15 × 15 μm pixels was used. Exposure times varied from 300 s for bright A- and B-type stars up to 3600 s for faint M-type dwarfs, yielding a signal-to-noise ratio (per spectral bin of 0.03 Å size) of typically 20 to 50, except for several F- and G-type stars used for the metallicity determination, which were exposed longer to achieve a S/N of 100 to 150. Radial velocity standard stars were observed at the beginning and end of each night. Flatfields and ThAr calibration exposures were taken before and after each observation night.

Altogether, we took spectra of 30 late-type and 9 early-type candidate members of NGC 2451 A and B, and of the late-type supergiant c Pup. All stars observed are listed in Table 1. Short exposures of the early-type stars and of c Pup were mainly taken in order to better define the mean radial velocity of the clusters. The objects X156 and X177 turned out to be visual binaries with angular separations of 4.0 and 4.4 arcsec, respectively. In both cases, spectra of both components were taken.

Data reduction has been performed by means of the FEROS Data Reduction pipeline within MIDAS. Briefly, the following procedures were applied: determination and subtraction of interorder background, straightening and extraction of echelle orders, removal of blaze function and correction of pixel-to-pixel variation (flatfielding), rebinning to wavelength and calibration, correction of the wavelength scale to barycentric values, and merging of the echelle orders to single 1D spectra. The FEROS spectrograph has two fibre entrances of which one is set to the star and one to the background sky, the two spectra are extracted separately.

To provide an idea of the quality of our data, we plot in Fig. 1 some examples of our spectra showing the region around the Li 6708 Å resonance line.

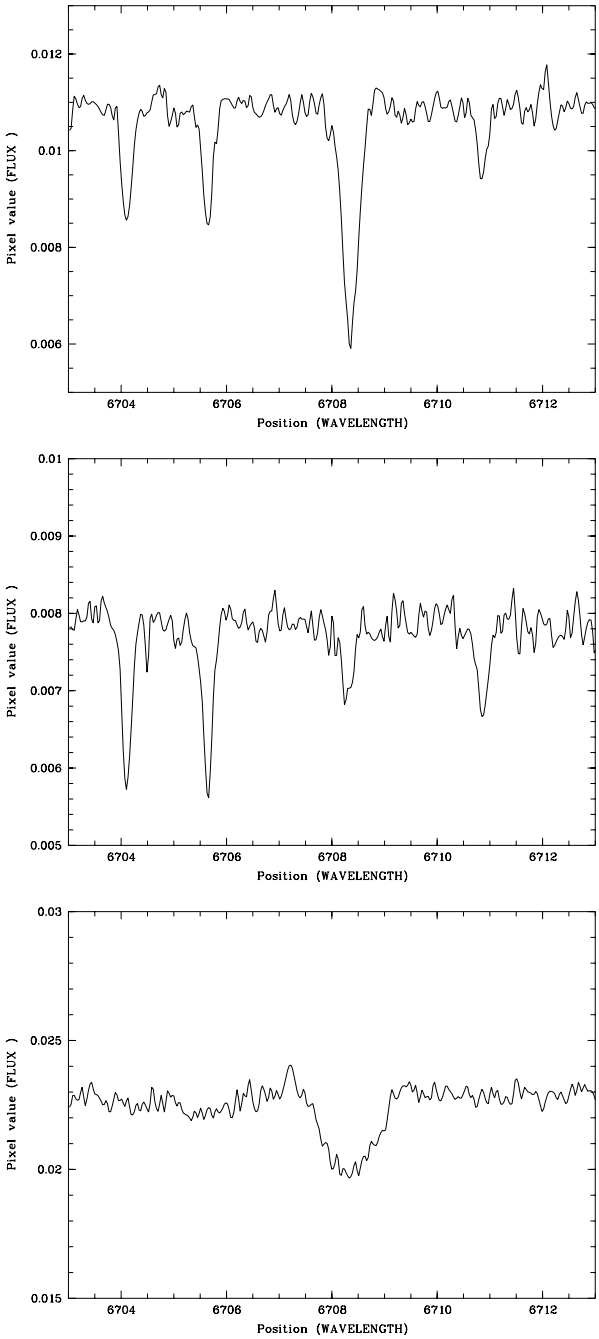

Fig. 1. Lithium 6708 Å line in the three NGC 2451 A stars (from top to bottom) X106, X114, X156A, illustrating the various shapes and strengths of the profiles.

3. Data analysis

3.1. Radial velocities

Radial velocities were measured by means of two different methods: i) Gauss-centering of selected (i.e., non-blended, moderately strong) Fe I and Ca I lines in the wavelength ranges 6000–6070 Å, 6410–6475 Å, and 7400–7450 Å; ii) cross-correlation within the same wavelength ranges as above, using a well-exposed solar spectrum (twilight sky) as a template. For stars with very broad spectral lines we convolved the solar template spectrum with a suitable Gauss function. Zero points for each night were set by observations of two radial velocity standard stars (HR 1829 and HR 4540). The night-to-night variations of the standard stars are typically 0.1–0.2 km s^{-1}.

A comparison between these two methods revealed that cross-correlation yields more accurate values only in case of low-S/N spectra. In most of the spectra, especially in those

Table 1. Candidate members of NGC 2451 A (upper part) and B (lower part), of which high-resolution spectra were taken. Magnitudes, de-reddened colours, spectral types, and X-ray parameters are taken from HWS.

X#	W#	Name	V	$(B-V)_0$	Spec.	$\log L_x$	$\log \frac{L_x}{L_{bol}}$	RV (km s^{-1})	$v \sin i$ (km s^{-1})	Notes
X3			10.66	0.51	F8V	28.88	−4.92	+23.0	21	
X11	256	HD 63079	6.91	–0.06	B9V	29.38	−6.01	+32.6:		non-member
X30			13.15	1.05	K4V	29.04	−3.99	+40.5	4	non-member
X31	68	CD–37 3870	11.46	0.64	G3V	29.91	−3.65	+23.6	15	
X40			15.49	1.37	K8V	28.99	−3.31	+23.1	8	
X61	251	HD 62991	6.53	–0.12	B3IV	–	–	+26.0		
X63	15	CD–37 3823	10.57	0.51	F8V	29.19	−4.68	+15.8	12	non-member
X72			12.38	0.75	G8V	29.74	−3.45	+12.4	22	non-member
X80	267	HD 63215	5.87	–0.10	B7V	29.38	−6.54	+24.8		
X103	244	HD 62876	8.62	0.11	A3V	29.55	−5.06	+26.2		
X106			12.30	0.80	K0V	29.46	−3.77	+23.4	7	
X108			14.57	1.36	K8V	28.82	−3.88	+53.7	5	non-member
X109	46	CD–37 3853	9.80	0.53	F8V	28.80	−5.29	+36.5	20	non-member
X114			12.71	0.88	K1V	28.52	−4.65	+23.4	7	
X116	50	CD–37 3859	10.01	0.41	F5V	28.82	−5.22	+20.0:	42	
X117			12.54	0.85	K1V	30.06	−3.09	+ 9.9	27	non-member
X132	47	HD 62974	8.30	0.14	A3V	29.77	−4.96	+22.6:		
X134	3	CPD–37 1499	10.84	0.55	F8V	29.42	−4.34	+21.0:		SB2
X142	89	CD–37 3897	10.01	0.51	F8V	29.69	−4.37	+25.7	11	
X149	94	CD–37 3902	9.46	0.42	F5V	29.27	−5.04	+20.3:	18	
X151			15.34	1.38	M0V	29.65	−2.73	+18:	65:	SB?
X156A	57	CD–37 3862	11.42	0.52	F8V	30.31	−3.38	+22.3:	59	binary
X156B	57	CD–37 3862	11.00	0.55	F8V	30.31	−3.38	+20.7	33	binary
X157	233	HD 62712	6.35	–0.10	B9Vsp	29.19	−6.51	+17.7		
X177A			11.29	0.60	G0V	30.27	−3.32	+22.9	14	binary
X177B			11.41	0.67	G5V	30.27	−3.32	+57.5	18	binary, SB
X181			13.55	1.10	K4V	29.61	−3.21	+21.2	23	
X187			12.58	0.83	K0V	29.81	−3.31	+22.8	10	
X188			10.95	0.60	G0V	30.09	−3.64	+22.4:	115	
X16	41	CD–37 3850	10.70	0.24	A8V	28.92	–5.40	–4.1		non-member
X33			12.76	0.63	G2V	29.67	–3.87	+14.8	21	
X42		CD–37 3910	11.50	0.40	F5V	30.37	–3.64	+12.3:	50	
X45	61	CPD–37 1565	11.83	0.51	F8V	29.69	–4.20	+15.1:	50	
X65			13.22	0.71	G8V	29.73	–3.64	+15.2	10	
X68			13.40	0.71	G8V	30.17	–3.13	+17.2:	62:	
X74			13.41	0.73	G8V	30.07	–3.23	+13.4	19	
X94	254	HD 63032 = c Pup	3.64	1.67	K2.5Ib-II	29.78	–8.72	+16.6		
X105	48	CPD–37 1549	11.65	0.44	F5V	29.91	–4.04	+16::	140::	
X119	2	CD–37 3810	10.30	0.23	A8V	29.76	–4.71	+10.0		
X139	266	HD 63216	8.61	–0.13	A0IV	29.55	–5.85	+10.5		

where the lines were sharp and well measurable, we prefered the method of measuring up to 15 individual lines and calculating the mean value. The formal error of our radial velocity values depends strongly on line widths and S/N and varies between 0.2 and 2 km s^{-1}. Only the values marked in Table 1 with a colon are less accurate with errors up to 5 km s^{-1} for late-type stars and 8 km s^{-1} for early-type stars. The systematic error is probably very low, given the very good reproduction of the standard star velocities. We assume that they do not exceed a few tenth of a km s^{-1}.

The resulting radial velocities are given in Table 1. Rejecting stars with more than about ±5 km s^{-1} deviation from the cluster mean, we derived mean radial velocities of +22.7 (±0.5) km s^{-1} for NGC 2451 A and +14.0 (±0.8) km s^{-1} for NGC 2451 B, while the velocity dispersion (i.e., formal standard deviation) is 2.3 km s^{-1} for cluster A and 2.5 km s^{-1} for cluster B. The stars assumed to be non-members of the clusters on the basis of radial velocity are indicated in the last column of Table 1. Note that X177B has been classified as a cluster member in spite of its high radial velocity. As will be pointed out

in detail in Sect. 4.1.1, the star turned out to be a spectroscopic binary.

Our radial velocity values are in very good agreement with Platais et al. (2001) who find +22.9 km s^{-1} for NGC 2451 A and +14.9 km s^{-1} based on six stars for NGC 2451 B.

3.2. Rotational velocities

Rotational velocities were measured by fitting the observed line profiles with synthetic profiles calculated from the spectrum synthesis (for details see Sect. 3.3.2). In principle, the shape of the synthetic profile resulting from the model atmosphere and the line formation program depends on a variety of broadening mechanisms: thermal broadening, microturbulence, macroturbulence, and projected rotation ($v \sin i$). The latter parameter is incorporated in the line formation code according to Unsöld (1955).

When fitting the observed profile with a synthetic profile, one has to take into account the broadening by the limited instrumental resolution. In order to estimate the contribution of the instrumental profile we calculated a synthetic profile of a heavy element line (barium 6141.7 Å), which is little influenced by thermal broadening, and set rotation, micro- and macroturbulence to zero. We then fitted the synthetic line to an observed telluric line (oxygen molecule lines around 6280 Å) which essentially reflects the pure instrumental profile, and adjusted only the macroturbulence as a proxy broadening parameter to achieve a good fit. The instrumental broadening turned out to be 3 km s^{-1}, which was subtracted quadratically from the $v \sin i$ values resulting from the fit of the stellar profiles. For example, a fit of the solar spectrum yields a formal value of $v \sin i = 4$ km s^{-1}, which is to be reduced by the instrumental broadening to the true value of 2 km s^{-1}. Given the small amount of the instrumental broadening this procedure is of sufficient accuracy, as test calculations have shown.

For the determination of rotational velocities we used the neutral iron lines at 6003, 6024, 6056, 6065, and 6412 Å, and the Ca I line at 6439 Å, which are quite strong yet not saturated lines and essentially not blended by nearby other lines. The uncertainty strongly depends on the signal-to-noise ratio of the spectra and on the rotational velocity itself. From the scatter between the different lines of a given star we estimate the probable $v \sin i$ error to be 1–2 km s^{-1} for stars with $v \sin i \lesssim 25$ km s^{-1} and up to 5 km s^{-1} for the faster rotating stars. So, the uncertainty in projected rotational velocities may be typically 10% of the derived value. The measured and reduced $v \sin i$ values of the observed late-type stars are listed in Col. 10 of Table 1.

3.3. Abundances

For consistency with previous investigations we estimated effective temperatures by means of the colour-temperature-relation given by Soderblom et al. (1993)

$$T_{\rm eff} = 1808(B-V)_0^2 - 6103(B-V)_0 + 8899$$

which is applicable up to $B - V < 1.4$; the temperatures are listed in Table 4. A surface gravity $\log g = 4.5$ was assumed for all the sample stars, while the microturbulence velocity was adjusted according to the relation

$$\xi = 3.2 \times 10^{-4}(T_{\rm eff} - 6390) - 1.3(\log g - 4.16) + 1.7$$

as given by Boesgaard & Friel (1990). Finally, the macroturbulence was set between 6 km s^{-1} for early F-type stars and 2 km s^{-1} for mid G-type and later stars according to Gray (1992).

We assume typical random errors of ±200 K in $T_{\rm eff}$, ±0.2 dex in $\log g$ and ±0.3 km s^{-1} in ξ.

3.3.1. Metallicity

For the metallicity determination we used well-exposed ($S/N \approx 100$) spectra of the F- and G-type stars listed in Tables 2 and 3. In each of the spectra we measured the equivalent widths (EWs) of a subset of Fe I lines chosen among 22 lines included in the range between 6315 Å and 7585 Å (see Table 2). Because of the very different appearance of the Fe lines in different stars owing to rotational velocities and S/N ratio, the number of measurable lines ranges between 7 and 17 and fewer lines were measured for only three stars (X156B, X42, and X45). Iron abundances were then derived by means of an LTE lines analysis using the MOOG code (Sneden 1973 – version December 2000) and Kurucz (1995) model atmospheres. We adjusted $\log gf$ values by carrying out an inverse abundance analysis of the solar spectrum observed with FEROS; we assumed $\log \epsilon(\mathrm{Fe})_\odot = 7.52$ and the usual solar parameters $T_{\rm eff\odot} = 5770$ K, $\log g_\odot = 4.44$, and $\xi_\odot = 1.1$ km s^{-1}.

The derived Fe abundances and their formal random errors are given in Table 3. For each star, the error includes the standard deviation in the mean from the different lines (σ_1 – which is a good approximation of the random error due to errors in the measured equivalent widths) and the random error due to the uncertainties in stellar parameters (σ_2). The latter was estimated by varying one parameter at the time and leaving the other two parameters unchanged; the errors due to each parameter were then quadratically added. Systematic errors are more difficult to estimate (see below). For most stars, we do not have enough lines for a spectroscopic determination of the microturbulence; the microturbulence relation as given above might introduce a systematic error, but we used it to be consistent with other cluster metallicity studies. We note, however, that for the stars with a sufficiently large number of measurable lines we did not find any major iron abundance vs. EW or EP trend, thus suggesting that our temperature and microturbulence scales are not largely in error. In addition, as mentioned, we carried out a differential analysis with respect to the Sun, and thus systematic uncertainties due to, e.g., atomic parameters and/or model atmospheres do not affect the inferred [Fe/H] values. We note that the microturbulence we have assumed for the Sun is in agreement with the expression that we have used for our sample stars; furthermore, if we assume a larger/smaller microturbulence (1.4/0.8 km s^{-1}) we would find a significant trend of abundances vs. EW.

As mentioned, for X156B in cluster A and X42 and X45 in cluster B only few lines were measurable (five, two and three, respectively) and thus the inferred iron abundances are quite

Table 2. Measured Fe I equivalent widths in mÅ.

λ (Å)	Sun	X31	X106	X114	X142	X149	X156B	X187	X33	X42	X45	X65	vB21	vB182
6315.81	42.5	–	53.3	54.8	–	–	–	–	–	–	–	–	57.2	56.2
6322.69	78.2	–	104.7	107.7	63.2	–	–	109.7	–	–	–	86.2	107.2	112.0
6330.85	34.9	–	41.8	43.5	27.2	–	–	–	–	–	–	–	49.8	48.0
6344.16	67.7	65.7	80.0	–	47.3	–	70.5	89.3	–	–	–	78.2	91.0	92.0
6380.75	53.4	53.5	58.2	60.5	45.7	–	45.5	62.7	53.8	–	–	56.0	–	–
6498.94	46.1	–	–	82.5	–	–	–	–	–	–	–	–	76.8	79.6
6593.88	85.5	–	–	–	–	–	–	–	–	–	–	107.7	116.4	122
6703.58	36.3	35.2	51.5	61.5	22.3	–	–	59.7	–	–	–	41.2	58.4	61.0
6710.32	16.7	–	–	40.3	–	–	–	–	–	–	–	–	39.0	–
6726.67	48.0	45.8	52.5	64.3	38.8	21.5	–	55.3	–	–	–	50.7	68.3	65.0
6733.15	28.0	27.7	–	–	19.2	12.0	–	–	–	–	–	38.8	43.2	41.6
6750.16	76.3	68.3	97.2	94.8	60.2	–	60.0	101.7	61.7	66.5	45.7	90.0	102.6	106.6
6786.86	27.7	–	33.2	39.8	–	9.0	–	–	–	–	–	–	44.0	–
6806.86	36.3	–	50.5	53.5	–	–	–	62.2	–	–	–	43.3	55.9	–
6810.27	50.8	50.0	62.8	–	40.8	23.7	49.2	69.5	57.2	–	47.0	57.7	–	–
6820.37	42.3	–	48.5	49.0	32.7	21.2	–	51.8	–	–	–	44.3	–	–
6828.60	56.6	–	–	–	–	–	–	–	73.2	66.3	–	–	–	–
6843.65	62.1	68.5	71.8	75.8	52.5	–	–	70.2	–	–	–	71.8	–	–
6858.15	52.6	–	60.3	67.3	34.7	31.7	–	–	39.7	–	–	49.8	–	–
7219.68	44.7	–	61.5	–	–	–	–	–	–	–	–	–	–	–
7443.03	40.4	–	47.8	–	53.7	–	–	–	–	–	–	–	–	–
7507.27	62.3	50.5	47.8	70.3	71.5	32.3	69.3	73.7	54.2	–	53.2	68.7	–	–
7583.80	84.7	–	–	110.7	–	–	–	–	–	–	–	90.5	–	–

Table 3. Derived iron abundances for selected stars of the NGC 2451 A and B clusters.

Cl.	X#	ϵ(Fe)	$\pm\sigma_1$	$\pm\sigma_2$
A	X31	7.46	0.09	0.16
A	X106	7.48	0.07	0.12
A	X114	7.51	0.08	0.09
A	X142	7.59	0.04	0.14
A	X149	7.42	0.06	0.14
A	X156B	7.67:	0.17	0.16
A	X187	7.54	0.08	0.11
B	X33	7.48	0.23	0.15
B	X42	8.1:	0.1:	0.14
B	X45	7.5:	0.2:	0.16
B	X65	7.50	0.09	0.16
NM	X63	6.97	0.13	
NM	X109	7.64	0.15	

uncertain. Also note that for X63, already rejected from cluster membership on the basis of radial velocity, a significantly lower iron abundance has been derived, supporting non-membership.

The weighted mean value for NGC 2451 A is ϵ(Fe) = 7.51 ± 0.08, while for NGC 2451 B we can only assume that the value is similar, yet rather uncertain. If we exclude X156B, we obtain ϵ(Fe) = 7.50 ± 0.08 for NGC 2451 A. Both clusters thus seem to have a metallicity very close to solar, contrary to early estimates based on photometry. A first hint on near-solar or even slightly super-solar metallicity of NGC 2451 has already been given by Margheim et al. (2000).

For an assessment of the systematic uncertainties affecting our analysis we determined the metallicity of two members of the Hyades cluster in the same fashion as for our sample stars: we analyzed the spectra of the stars vB21 and vB182, which were observed with UVES on VLT UT2 (at a similar resolution as that of our spectra) during a different program. We used the same $T_{\rm eff}$ vs. color calibration and the same expression to derive ξ, obtaining $T_{\rm eff}$ = 5141 K, ξ = 0.86 km s^{-1} and $T_{\rm eff}$ = 5079 K, ξ = 0.84 km s^{-1} for vB21 and vB182, respectively. A gravity log g = 4.5 was assumed for both stars. The *EW*s of the Fe I lines measured in the spectra of the two Hyades members are listed in Table 2 (fewer lines are available for the Hyades stars due to the smaller spectral range), together with those of NGC 2451 AB stars. Note that, as done for NGC 2451, we excluded from the analysis the lines that would give an abundance >1σ different from the mean value. For both vB21 and vB182 we obtained ϵ(Fe) = 7.62 ± 0.03, or [Fe/H] = +0.10 ± 0.03, to be compared with the commonly quoted value for the Hyades [Fe/H] = +0.13 (Boesgaard & Budge 1989). This indicates that the systematic errors affecting our analysis should not be too large and confirms that both NGC 2451 clusters have a metallicity close to solar.

3.3.2. Lithium abundances

For the determination of lithium abundances we used two different methods. The usually applied method is to measure equivalent widths which, in combination with effective temperatures, yield the Li abundances utilizing curve-of-growth (COG) tables. We also applied a different method by using synthetic spectra calculated from model atmospheres and line

Table 4. Results of detailed spectral analysis: lithium equivalent widths and derived abundances, Hα appearance and effective temperatures.

X#	$T_{\rm eff}$ (K)	EW(Li) (mÅ)	σ_{EW} (mÅ)	$\epsilon(\mathrm{Li})_{\rm COG}$	$\epsilon(\mathrm{Li})_{\rm Syn}$	Hα profile	EW(K) (mÅ)	Notes
X3	6343	130	4	3.31 ± 0.08	3.50		133	
X30	4484	11	1	−0.31 ± 0.15	0.35		210	
X31	5734	174	3	3.02 ± 0.10	3.25		191	
X40	3931				<0.00	emission	245	
X63	6257	67	3	2.78 ± 0.09	2.85		77	
X72	5339	191	6	2.69 ± 0.12	3.05	emission	233	
X106	5174	165	3	2.42 ± 0.12	2.57		226	
X108	3943				<0.20	pec, PCyg	217:	
X109	6172	21	3	2.01 ± 0.11	2.30		136	
X114	4928	37	2	1.20 ± 0.13	1.35		245	
X116	6701	89	6	3.32 ± 0.10	3.47		87	
X117	5018	272	3	2.81 ± 0.13	3.15	emission	331	
X134	6089	61:	3:	2.58: ± 0.09	2.47:		146:	double profiles (SB2)
X142	6257	70	2	2.87 ± 0.08	2.95		140	
X149	6609	62	2	3.03 ± 0.08	3.10		115	
X151	3910				<0.50	emission	1000:	
X156A	6214	100	3	3.01 ± 0.08	3.10		128	
X156B	6089	146	5	3.20 ± 0.09	3.50		204	
X177A	5888	160	3	3.09 ± 0.10	3.30		170	
X177B	5585	194	3	2.99 ± 0.11	3.30		166	
X181	4373	268	4	1.86 ± 0.12	2.25	emission	435	
X187	5079	203	3	2.52 ± 0.13	2.75	filled	249	
X188	5928	167	15	3.18 ± 0.12	3.00	core em.		K not measurable
X33	5772	173	6	3.07 ± 0.11	3.15		184	
X42	6747	152	7	3.79 ± 0.09	3.90		149:	
X45	6257				2.30:			Li and K EWs not measurable
X65	5477	166	3	2.70 ± 0.11	3.10	core em.	242	
X68	5477	136	40	2.53 ± 0.26	2.90	emission	252	
X74	5407	212	3	2.90 ± 0.12	3.20	emission	257	
X105	6564					core em.		Li and K EWs not measurable

formation spectrum synthesis. The former method provides results comparable to previous studies of other clusters achieved in the same way. The latter has the advantage of fitting the whole profile, i.e., including possible blends by other spectral lines.

Curves of growth – Lithium LTE abundances were derived from measured EWs of the 6707.8 Å Li I doublet using the COG tables of Soderblom et al. (1993) which cover a temperature range from 4000 to 6500 K. For stars outside of this range we extrapolated the COG tables following Soderblom et al. (1999). NLTE corrections were not applied since they are typically of the order 0.1 dex, i.e., within the errors (see, e.g., Randich et al. 2001). As is well known, a Fe I feature (λ = 6707.4 Å) lies close to the Li doublet; for most of the slow rotators in our sample ($v \sin i < 12$ km s^{-1}) this feature was separated from the Li line, while for the other stars it was blended. In all these cases, we corrected the measured Li EWs using the approximation of Soderblom et al. (1993) for the Fe line, namely: $EW(\mathrm{Fe}) = 20 \times (B-V)_0 - 3$ mÅ. Errors in derived abundances were estimated by quadratically adding the error due to the uncertainty in Li EWs and the error due to the uncertainty in $T_{\rm eff}$.

The measured Li equivalent widths, their corresponding errors, and the Li abundances derived by the COG method are listed in Cols. 3–5 of Table 4, respectively.

Spectrum synthesis – First, we calculated $T-\tau$–relations with the model atmosphere code ATLAS9 (Kurucz 1992) using $\log g = 4.40$ and mixing lengths $\alpha(T_{\rm eff}, \log g)$ adopted from Ludwig et al. (1999). However, since ATLAS9 models do not reproduce the temperature stratification in the outer atmospheres correctly and yield too low temperatures, the derived Li abundances were at first considerably underestimated (up to ∼1 dex).

We instead used an empirical Holweger-Müller (1974) solar model ($\log g = 4.4$), after applying linear scaling to the respective effective temperatures of our sample stars. This is of sufficient accuracy for the temperature regime of the stars analyzed. Based on the $T-\tau$–relations we carried out an LTE-abundance analysis using the Kiel line formation code LINFOR (see Holweger & Rentzsch-Holm 1995, and

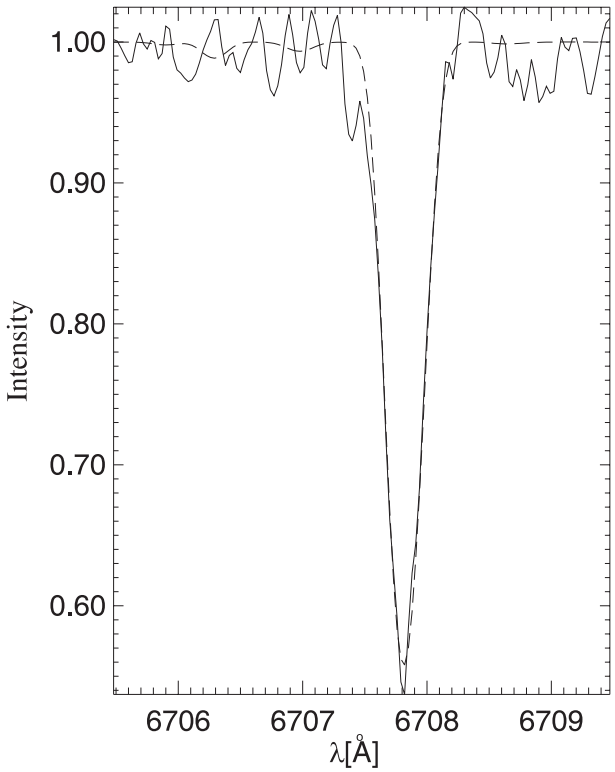

Fig. 2. Fit of a synthetic spectrum (dashed line) to the observed Li 6708 Å profile (solid line) of X106.

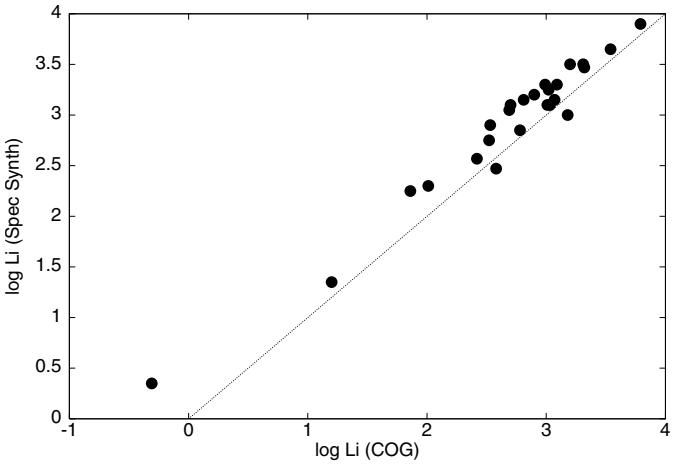

Fig. 3. Comparison between Li abundances derived by curve-of-growth techniques and spectrum synthesis.

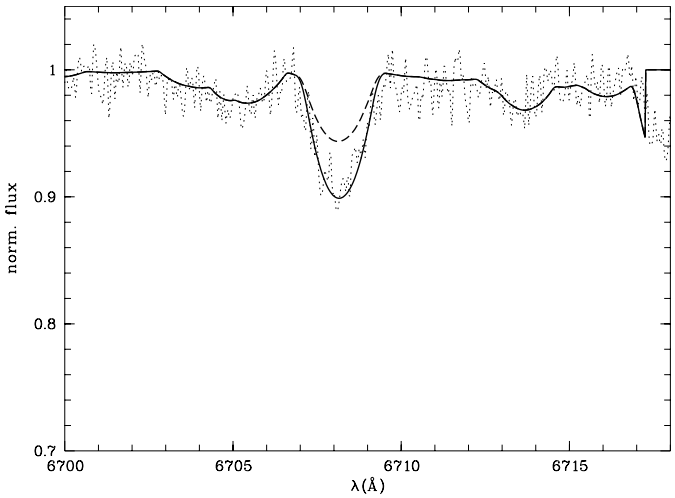

Fig. 4. Observed (dotted line) and synthetic spectra of X42. The synthetic spectra were obtained with a metallicity [Fe/H] = +0.3 and Li abundances equal to 3.3 (dashed line) and 3.75 (solid line).

references therein). Atomic data were taken from the Kurucz compilation (1994). $v \sin i$ and chemical abundances were then varied until a satisfactory fit could be achieved. An example of a fit of a synthetic Li 6708 Å line to the observed profile is shown in Fig. 2.

The uncertainties in Li abundances from the synthetic spectrum fits are of the order 0.05 to 0.1 dex, in a few cases of fast rotating stars and low S/N up to 0.2 dex. This does not include any systematic errors resulting from temperature and other parameter uncertainties. We have to keep in mind that the scaled Holweger-Müller atmosphere is correct only for stars close to the solar temperature, and that deviations are increasing with increasing temperature difference to the Sun.

The lithium abundances derived from spectrum synthesis are given in Col. 6 of Table 4. In general, the agreement with the COG values is quite satisfactory, the synthesis values lying typically 0.1–0.3 dex higher (see Fig. 3). Only at the lower end of the temperature regime the deviations become larger (up to 0.5 dex).

Finally, as an additional check of the very high Fe and Li abundances found for X42 (see Tables 3 and 4), for this star we carried out a full spectral synthesis using MOOG; the comparison between the observed spectrum and two synthetic spectra obtained with log n(Li) = 3.3 and 3.75 is shown in Fig. 4. The figure clearly confirms that X42 has a lithium abundance much above the meteoritic value. Furthermore, the best fit was obtained with a metallicity [Fe/H] = +0.3 which is somewhat below the value derived from equivalent widths, but still significantly higher than that of the other cluster members.

4. Discussion

It is important to keep in mind that the sample of spectroscopically observed stars is X-ray selected and, hence, biased towards X-ray active and thus more rapidly rotating stars. However, such a bias would not affect the pattern of Li abundances among the F/G-type stars since no Li–rotation correlations have been found for such stars in other young clusters. In addition, the X-ray survey covers only part of cluster NGC 2451 A and does not include the assumed cluster center. As discussed by HWS, it is difficult to estimate the completeness of the X-ray selected sample given the sparseness of sufficiently deep proper motion surveys. While in the central part of the X-ray surveyed region the sensitivity is probably large enough to identify about 80% of the members, this fraction decreases to 50–60% in the outer regions. This holds at least for the brighter (i.e., F- and G-type) stars, which are included in the astrometric study by Platais et al. (2001). For the K- and M-type dwarfs the X-ray selected sample is probably much less

complete, as their X-ray emission is constrained by the well-known saturation limit.

4.1. Improved membership

While all of the target stars selected for spectroscopy have been considered as member candidates on the basis of X-ray emission and proximity to the cluster main sequences, radial velocity provides an additional rather stringent criterion for cluster membership. Due to measured *RV* values as given in Table 1 we assume all stars deviating by more than 5 km s^{-1} from the cluster mean values to be probable non-members, namely: X11, X30, X63, X72, X108, X109, X117, and X16. The star X63 can also be rejected according to its discordant iron abundance (see Sect. 3.3.1). All other stars for which we measured radial velocities can now be considered as *bona fide members* of NGC 2451 A and B.

In Table 4 we also list whether the Hα profile is seen in emission. Hα emission occurs in stars with strong chromospheric activity and is particularly strong in stars with a high L_X/L_{bol} ratio. Especially in the case of optically faint (i.e., rather late-type) stars, Hα emission is a good indicator that an X-ray source has been identified correctly with an active star.

However, as can be inferred from Tables 1 and 4, a few stars (X72, X108, X117) are present which show a strong degree of activity, both in Hα and X-rays, yet are not cluster members according to radial velocity. Either these stars are young field stars accidentally located in or near the cluster or they are members and SB1 binaries shifted in radial velocity by an unseen companion like X177B (see below).

4.1.1. Notes on individual stars

X134: all spectral lines show a double profile; the star is obviously an SB2 binary. No changes in radial velocity can be inferred from two spectra taken two nights apart.

X142: we do not have measured magnitudes and colours of our own since the star is overexposed in our CCD images. The $B - V$ colour listed in SIMBAD (0.33) is probably a transformed TYCHO measurement and differs considerably from the older photoelectric value by Williams (1967) which is 0.52. However, using the lower value and the corresponding higher temperature (7131 K) yields a metallicity of +0.6 dex and a lithium abundance above the meteoritic value. Furthermore, by assuming T_{eff} = 7131 K in the determination of metallicity, we would get a strong negative correlation between Fe abundances and excitation potential. We therefore believe the older value by Williams to be more reliable, yielding T_{eff} = 6257 K, and derive a lithium abundance of 2.87.

X156AB: the star turned out to be a close (4.0 arcsec) double barely resolved by the CCD images used for photometry. For both components spectra could be taken and both stars are members according to radial velocity.

X177AB: this object also turned out to be a close (4.4 arcsec) double. The radial velocity of component B seems to be much larger than the cluster mean, yet the Ca II H and K lines show two emission cores at radial velocities of ~+35 km s^{-1} and ~–56 km s^{-1}. Assuming the star to be a spectroscopic binary and a member of NGC 2451 A (i.e., having a center-of-mass radial velocity of ~–23 km s^{-1}), the mass ratio would be $M_1/M_2 \approx 1.8$. Given the colour of the optically dominating star, the primary may be an early or mid G-type star and the secondary (showing no photospheric lines lines in the spectrum) an early K-type star.

X105: the star shows extremely broadened spectral lines, hence the *RV* and $v \sin i$ values are very coarse.

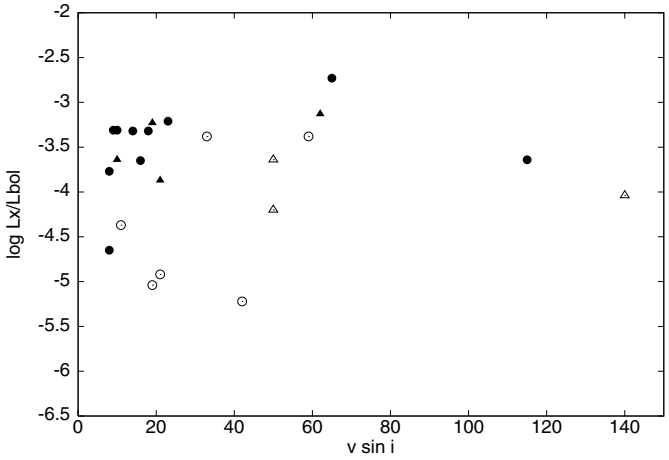

Fig. 5. Normalized X-ray emission vs. $v \sin i$ (in km s^{-1}). Circles denote NGC 2451 A members while triangles denote NGC 2451 B members. Open symbols represent F-type stars, while filled symbols are G- or K-type stars.

4.2. Rotation and activity

The dependence of activity measured by the normalized X-ray flux on rotation is illustrated in Fig. 5. Bolometric fluxes have been derived by applying bolometric corrections from Johnson (1966) according to the de-reddened $(B - V)_0$ colours of the stars. The symbols indicate to which cluster a star belongs and whether it has an F- or a later spectral type. While the G- and K-type stars follow the usual behaviour, i.e., a steep increase of X-ray luminosity with increasing rotational velocity until the saturation limit is reached of $\log L_X/L_{bol} \approx -3$ above $v \sin i \sim 20$ km s^{-1}, the F-type stars do not seem to follow this relation. In particular, there are stars like X116 which are relatively X-ray faint although rotating quite fast. The non-dependence of X-ray emission on rotation is well known for early F-type stars with very shallow convection zones (Walter 1983; Hünsch 2001), whereas the late F-type stars were assumed to behave like G-type stars.

Interestingly, there are two stars (X188 and X105) rotating extremely fast (>100 km s^{-1}) yet exhibiting X-ray emission significantly below the saturation limit. Here, we may have two additional examples of the supersaturation phenomenon first noted by Prosser et al. (1996) in the α Per cluster (see also Randich 1998).

In Fig. 6 we show the so-called Rossby diagram of the NGC 2451 clusters, i.e., the dependence of normalized X-ray emission on Rossby number, which is defined as the ratio

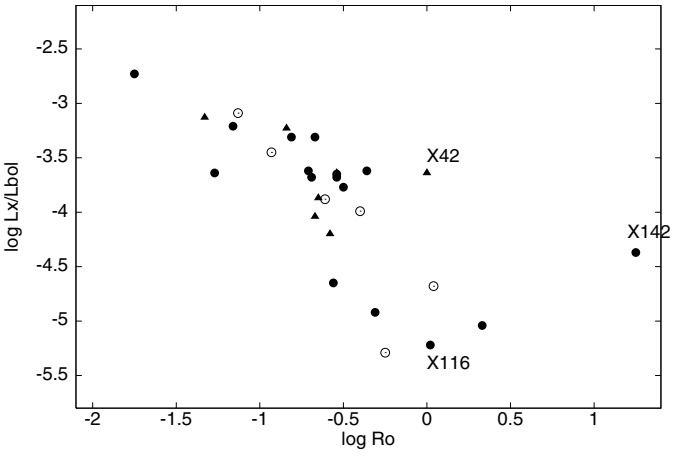

Fig. 6. Rossby diagram of NGC 2451 A (filled circles) and B (triangles) and non-members (open circles).

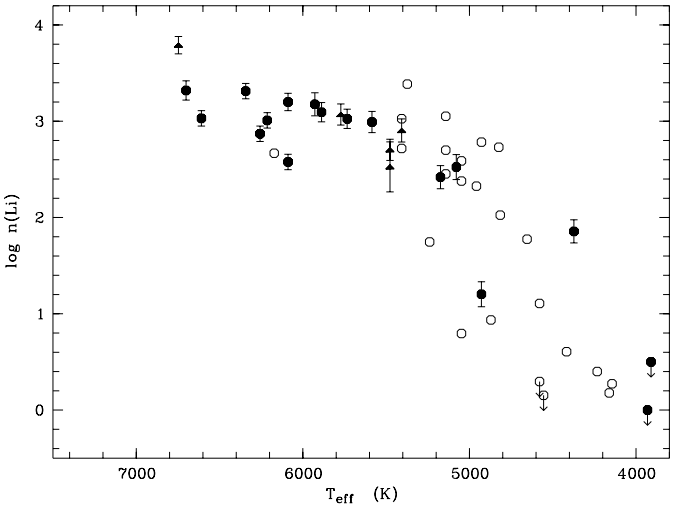

Fig. 7. Lithium abundances vs. effective temperature. Filled symbols represent NGC 2451 A (circles) or B (triangles) members, open symbols are stars of the α Per cluster.

of rotation period over convective turnover time (τ_c – see Noyes et al. 1984). We computed τ_c values following Noyes et al. (1984), while (upper limits on) rotational periods were derived from projected rotational velocities using stellar radii for main-sequence stars from Drilling & Landolt (2000). The Rossby diagram allows investigating the relationship between rotation and activity taking into account also the dependence of activity on spectral type and depth of the convective zone. It has been shown that the relation between Rossby number and L_X/L_{bol} is quite universal for late-type stars of different age and effective temperature, implying that the same activity-(rotation + convection) relationship holds for solar–type stars and stars with lower/higher masses and that such a relationship does not change with age (e.g., Randich 2000, and references therein).

The Rossby diagram for the NGC 2451 clusters is in agreement with previous findings: except for two outliers (X142 and X42, both F-type stars), which may be stars seen pole-on so that their rotation period could be overestimated, the stars of both clusters, as well as the non-members, nicely follow the pattern seen in other clusters. Note that X116, which was deviant in the $\log L_X/L_{bol}$ vs. $v \sin i$ diagram, is within the mean trend of the other stars in the Rossby diagram.

4.3. Lithium abundances

In Fig. 7 we plot the Li abundances as a function of effective temperature for our sample stars (filled circles and triangles for clusters A and B, respectively) and α Per (open circles). Li abundances for this cluster were re-derived consistently with our sample stars after retrieving Li equivalent widths from the studies of Balachandran et al. (1996) and Randich et al. (1998). The figure shows that the Li vs. T_{eff} distributions of clusters A and B are very similar and that both are similar to the distribution of α Persei, consistent with the assumption that NGC 2451 A and B and α Per have similar ages, as already suggested by the isochrone fits and the mean X-ray luminosities (see HWS). As in α Per, stars warmer than the Sun have undergone very little Li depletion and show a rather tight Li vs. T_{eff} pattern. Although our sample is extremely small below 5200 K, the cooler stars show some amount of Li depletion and, if we assume X114 to be a member, a star-to-star scatter in Li may be present among the cooler stars. There is, of course, no definite possibility to confirm the membership of X114, yet its position on the main sequence, metallicity and radial velocity are all in very good agreement with the cluster means, hence non-membership seems to be rather unlikely.

As mentioned in the introduction, a dispersion in Li abundances, which was first detected in the Pleiades (Soderblom et al. 1993), is seen among K-type stars in several young clusters; the presence of a dispersion among otherwise similar stars suggests that the amount of Li depletion is determined by some additional parameter besides mass, age, and chemical composition. Based on the high Li – fast rotation relationship (which however breaks down for stars cooler than ~4500 K, see García López et al. 1994), the most popular parameter is stellar rotation and/or pre-main sequence (PMS) rotational history, with Li depletion being driven by rotationally induced mixing. As an alternative explanation, several authors investigated whether the scatter in Li *EW*s could be due to the effects of high surface and chromospheric activity on the formation of the Li line rather than to a genuine spread in abundances (e.g., Jeffries 1999; Stuik et al. 2000; Barrado y Navascués et al. 2001; Randich 2001).

We have only very few stars cooler than 5000 K to put additional statistical empirical constraints on the dispersion and its relationship with rotation. We note however that the three stars in our sample with T_{eff} around 5000 K (X106, X114, and X187) are all slow rotators ($v \sin i \leq 10$ km s^{-1}), but have different levels of activity, with X114 being significantly less active than the other two stars. X114 is also the Li-poorest star among the three. In other words, given the activity-rotation relationship, X106 and X187 are presumably more rapid rotators seen at a small inclination angle and the high rotation/activity – high Li relationship seems to hold also for NGC 2451.

In order to further investigate whether the dispersion in Li is a real dispersion in abundances, we measured the *EW*s of

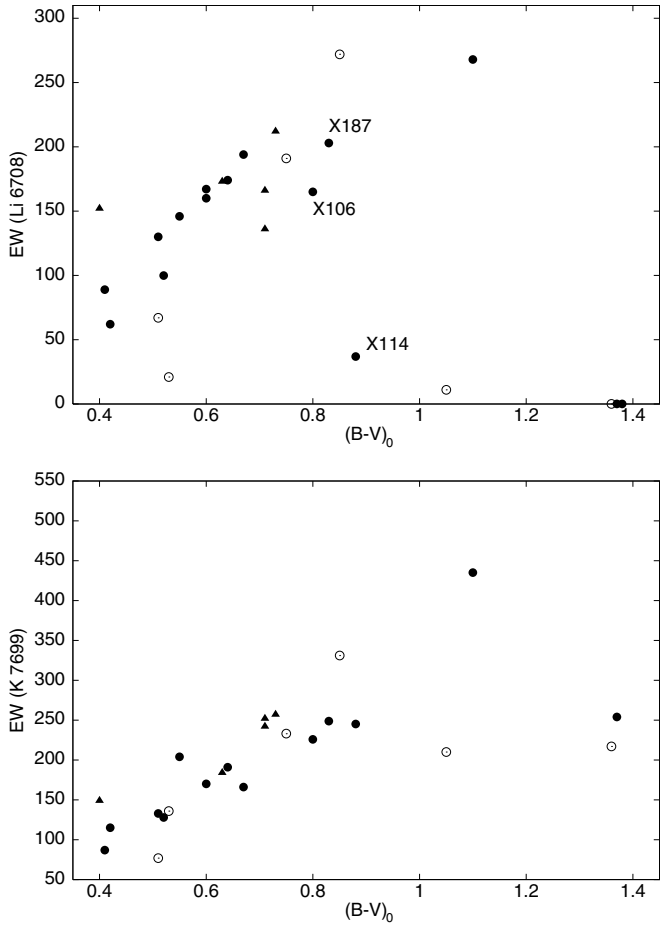

Fig. 8. Li 6708 Å (*top*) and K 7699 Å (*bottom*) equivalent widths vs. de-reddened $B-V$ colour. Symbols as in Fig. 6.

the K I 7699 Å line (Col. 8 in Table 3). As discussed in previous studies, the formation conditions of this line are very similar to those of the Li I 6707.8 Å line, but potassium is not destroyed in stars. Thus, if activity affects Li *EW*s and the Li vs. color pattern, a similar effect should be clearly seen in the K vs. color distribution (e.g., Jeffries 1999; Randich 2001). In Fig. 8 we plot lithium and potassium equivalent widths as a function of dereddened $B-V$ color; the figure shows that above $(B-V)_0 \gtrsim 0.7$ the lithium *EW*s exhibit a strong scatter from star to star, while the potassium *EW*s seem to follow a much tighter relation, and significant scattering only appears to be present among the coolest stars ($(B-V)_0 > 1.0$). We note in particular that the three stars X106, X114, and X187 have very similar K I equivalent widths, which suggests that the latter are not affected by activity; this in turn implies that the scatter in Li *EW*s in NGC 2451 possibly reflects a true abundance scatter. On the other hand, a scatter in potassium may be present among the coolest cluster stars, for which, however, we were able to measure only upper limits in Li abundances.

We finally note the very high Li abundance of X42 in cluster B, a factor of about three higher than the meteoritic value. Although based on very few lines only, this star also seems to show a significantly enhanced Fe abundance with respect to the other cluster members. Note that a high [Fe/H] value is found with spectral synthesis as well. It is surprising that this star lies almost exactly on the cluster main-sequence and shows a radial velocity consistent with cluster membership. If the high metallicity is true, and given its observed colour, the star would be ≈350 K hotter than listed in Table 4 calculated for the mean cluster (i.e., solar) metallicity. Then, the Li abundance of X42 would be even higher!

The discovery of a super-Li rich star in the Hyades-age cluster NGC 6633 was recently reported by Deliyannis et al. (2002); besides having a very high Li content (a factor of 10 higher than meteoritic), they also found this star to be overabundant in Fe and Ni and underabundant in C; they interpreted the high Li as the proof of the action of diffusion. Richer & Michaud (1993) indeed predict that, for stars in a narrow temperature range ($T_{\rm eff}$ between 7100 and 6900 K – the so-called "Li-peak"), lithium should be accelerated upwards, enriching the surface convective zone. Assuming an enhanced metallicity for X42 (see above), the star would be located exactly on the blue side of the Li peak. On the other hand, it rotates rather rapidly, possibly preventing diffusion due to meridional circulation (Charbonneau & Michaud 1991). Very recently, Laws & Gonzalez (2003) carried out a new analysis of the super-Li rich star in NGC 6633 and, based on the abundance pattern, concluded that accretion of circumstellar matter, rather than diffusion (which, according to them, is a secondary effect) is the best explanation for the observed abundance anomalies. Although, given the rapid rotation of X42, a detailed analysis providing the full abundance pattern is not feasible, accretion indeed appears as a viable explanation for the high Li and iron content of this star.

5. Conclusions

Complementing our preceding photometric and X-ray study (HWS) we have performed a detailed spectroscopic study of the NGC 2451 A and B clusters. The combination of these different observational approaches has led to the most comprehensive picture so far concerning membership of individual stars and the global properties of these nearby clusters.

On the basis of photometric data, X-ray emission, and radial velocities we can quite reliably identify probable cluster members, of which there are now 22 in NGC 2451 A and 10 in NGC 2451 B. An additional 10 stars of cluster A and 38 stars of cluster B can still be regarded as member *candidates*, yet we have no radial velocity information for them. The mean radial velocities for NGC 2451 A and B have been determined to be +22.7 km s^{-1} and +14.0 km s^{-1}, respectively.

The rather large number (6) of late-type stars originally regarded as member candidates on the basis of X-ray emission and photometry but rejected from cluster membership due to radial velocity is somehow surprising, in particular considering the fast rotation and large degree of activity of some of these stars. Additional spectroscopic observations are required to clarify whether these stars could be SB1 binaries with variable radial velocities.

Contrary to previous narrow-band photometric studies, both clusters (less certain for cluster B) have a metallicity close to the solar value. This demonstrates that photometric determinations of cluster metallicities should be regarded with

care, especially when membership of individual stars is not reliably known. The original aim to investigate the activity-rotation relation and the amount of Li depletion for a cluster of significantly different metallicity could thus not be achieved. However, in view of the limited number of clusters studied in detail, especially concerning the question whether a particular cluster can be regarded as representative, our data on the NGC 2451 clusters provide a valuable contribution to the existing database on open clusters.

Lithium abundances have been derived by two different methods, namely measuring equivalent widths and applying curve-of-growth techniques as well as fitting the observed spectral line profiles by synthesized spectra from model atmospheres. Although the latter method yields slightly higher Li abundances, the differences are mostly within the errors and the two methods can be assumed to be consistent. The spectrum synthesis also yields projected stellar rotational velocities after possible line profile broadening mechanisms have been taken into account. The overall pattern of Li depletion in NGC 2451 A and B is similar to that of the α Per cluster, consistent with the results from isochrone fitting and the X-ray luminosity distribution, and suggesting that the three clusters are about co-eval.

To find out whether the Li *EW*s do really represent the true abundances or are affected by some other mechanisms like activity, we also measured the potassium resonance line at 7699 Å which underlies similar line formation conditions as the lithium 6708 Å line. Although our data are sparse, we do not confirm the scatter in K *EW*s observed by Randich (2001) among the early K-type stars in IC 2602 and IC 2391; yet we find a significant scatter only for the coolest stars above $(B-V) \approx 1.0$. In this respect, an extension of spectroscopy towards fainter and cooler stars would be of great value.

Finally, a member of cluster B shows a significantly enhanced Li abundance for which, however, we do not have a viable explanation.

Acknowledgements. We would like to thank H. Holweger for discussions on the spectrum synthesis, O. Stahl for his kind help concerning the data reduction, and S. Moehler for helpful suggestions on the data analysis. We also thank the referee (R. D. Jeffries) for his useful comments on the manuscript. This work has been supported by the Deutsche Forschungsgemeinschaft (DFG) under grants HU 546/4-1 and HU 564/6-1 and by the Deutsches Zentrum für Luft- und Raumfahrt (DLR) under grants 50 OR 9617 and 50 OR 0005.

References

Balachandran, S. C., Lambert, D., & Stauffer, J. R. 1996, ApJ, 470, 1243
Barrado y Navascués, D., García López, R. J., Severino, G., & Gomez, M. T. 2001, A&A, 371, 652
Boesgaard, A. M., & Budge, K. G. 1989, ApJ, 338, 875
Boesgaard, A. M., & Friel, E. D. 1990, ApJ, 351, 467
Charbonneau, P., & Michaud, G. 1991, ApJ, 370, 693
Deliyannis, C. P. 2000, in Stellar Clusters and Associations: Convection, Rotation, and Dynamos, ed. R. Pallavicini, G. Micela, & S. Sciortino, ASP Conf. Ser., 198, 235
Deliyannis, C. P., Steinhauer, A., & Jeffries, R. J. 2002, ApJ, 577, L39
Drilling, J. S., & Landolt, A. U. 2000, in Allen's Astrophysical Quantities, 4th edition, ed. A. N. Cox (Springer-Verlag), 389
García López, R. J., Rebolo, R., & Martín, E. L. 1994, A&A, 282, 518
Gray, D. F. 1992, The Observation and Analysis of Stellar Photospheres, 2nd ed. (Cambridge Univ. Press), 416
Holweger, H., & Müller, E. A. 1974, Sol. Phys., 39, 19
Holweger, H., & Rentzsch-Holm, I. 1995, A&A, 303, 819
Hünsch, M. 2001, PASPC, 223, 967
Hünsch, M., Weidner, C., & Schmitt, J. H. M. M. 2003, A&A, 402, 571 (HWS)
Jeffries, R. D. 1999, MNRAS, 309, 189
Jeffries, R. D. 2000, in Stellar Clusters and Associations: Convection, Rotation, and Dynamos, ed. R. Pallavicini, G. Micela, & S. Sciortino, ASP Conf. Ser., 198, 245
Johnson, H. L. 1966, ARA&A, 4, 193
Kurucz, R. L. 1992, Rev. Mex. Astron. Astrofis., 23, 181
Kurucz, R. L. 1995, private communication
Kurucz, R. L. 1994, CD-ROMs, July 3, 1994 edition
Laws, C., & Gonzalez, G. 2003, ApJ, in press [arXiv:astro-ph/0306168]
Ludwig, H. G., Freytag, B., & Steffen, M. 1999, A&A, 346, 111
Lyngå, G., & Wramdemark, S. 1984, A&A, 132, 58
Margheim, S. J., King, J. R., Deliyannis, C. P., & Platais, I. 2000, BAAS, 196, 4210
Noyes, R. W., Hartmann, L., Baliunas, S. L., Duncan, D. K., & Vaughan, A. H. 1984, ApJ, 279, 763
Pasquini, L. 2000, in The Light Elements and their Evolution, ed. L. da Silva, M. Spite, & J. R. de Medeiros, IAU Symp., 198, 269
Platais, I., Kozhurina-Platais, V., Barnes, S., et al. 2001, ApJ, 122, 1486
Prosser, C. F., Randich, S., Stauffer, J. R., Schmitt, J. H. M. M., & Simon, T. 1996, AJ, 112, 1570
Randich, S., Martín, E. L., Garciía López, R. J., & Pallavicini, R. 1998, A&A, 333, 591
Randich, S. 1998, in The Tenth Cambridge Workshop on Cool Stars, Stellar Systems and the Sun, ed. R. A. Donahue, & J. A. Bookbinder, ASP Conf. Ser., 154, 501
Randich, S. 2000 in Stellar Clusters and Associations: Convection, Rotation, and Dynamos, ed. R. Pallavicini, G. Micela, & S. Sciortino, ASP Conf. Ser., 198, 401
Randich, S. 2001, A&A, 377, 512
Randich, S., Pallavicini, R., Meola, G., Stauffer, J. R., & Balachandran, S. C. 2001, A&A, 372, 862
Richer, J., & Michaud, G. 1993, ApJ, 416, 312
Sneden, C. 1973, ApJ, 184, 839
Soderblom, D. R., Jones, B. F., Balachandran, S., et al. 1993, AJ, 106, 1059
Soderblom, D. R., King, J. R., Siess, L., Jones, B., & Fisher, D. 1999, AJ, 118, 1301
Stuik, R., Bruls, J. H. M. J., & Rutten, R. J. 1997, A&A, 322, 911
Unsöld, A. 1955, Physik der Sternatmosphären (Berlin: Springer Verlag), 508
Walter, F. M. 1983, ApJ, 274, 794
Williams, P. M. 1967, Mon. Notes Astron. Soc. S. Afr., 26, 30